The Minkowski Overlap and the Energy Conserving Contact Model for Discrete Element Modelling of Convex Non-Spherical Particles

Y. T. Feng[1*] Yuanqiang Tan[2]
[1] Zienkiewicz Centre for Computational Engineering, Swansea University, UK
[2] The Institute of Manufacturing Engineering, Huaqiao University, China

Abstract

A unified contact overlap, termed the Minkowski overlap, between any two shapes is proposed in this paper. This overlap is based on the concept of the Minkowski difference of two shapes, and particularly on the equivalence between the contact state of the two shapes and the location of the origin relative to their Minkowski difference. The Minkowski contact features of a contact, including the overlap, normal direction and contact points, are also defined for convex shapes. In particular, an important property of the Minkowski overlap is introduced which lays the solid theoretical foundation for proposing a Minkowski overlap based energy-conserving contact model in the current work. The energy-conserving property for cases where the contact normal direction and point may be subject to discrete changes is also rigorously proved. For convex particles, the computational procedures combining both GJK and EPA algorithms are outlined, and uniqueness and ambiguity issues associated with some special cases are clarified and resolved. The elastic energy conservation of the proposed contact model for convex shapes in elastic impact is further verified using two numerical examples, and two more examples involving more convex particles with different sizes and shapes are also conducted to demonstrate the robustness and applicability of the proposed Minkowski overlap contact model and the computational procedures.

KEYWORDS: Minkowski overlap; GJK and EPA algorithms; Energy conservation; Convex polyhedral particle; Convex non-spherical particles

1 Introduction

The modelling of contact between arbitrarily shaped particles has been a major research theme in the discrete element method [1]. A comprehensive review of existing contact models for non-spherical particles can be found, for instance in [2] and references therein.

In almost all existing contact models for convex particles, including spheres and non-spherical shapes such as polyhedra [3], cylinders [4], super-quadrics [5], super-ellipsoids [6] and dilated particles [7, 8], the contact overlap has been the dominant contact feature that is adopted to define various normal contact models to compute contact forces. The main issue associated with these contact models is that the definition of the contact overlap for a pair of non-spherical particles is often established on an *ad-hoc* basis rather than based on a sound

*e-mail: y.feng@swansea.ac.uk

contact theory. Some possible adverse consequences of such an approach for modelling of general shaped particles are highlighted in [9].

The work of [9] is the first attempt to establish a generic *discrete element contact theory* for any shaped particles solely based on the contact energy conservation principle, from which different energy-conserving normal contact models can be derived when a contact energy function is defined in terms of contact features. A contact model derived in such a manner will provide robust and numerically stable computational procedures for any complex contact scenario, as demonstrated by using the contact volume based energy-conserving contact model presented in [10, 11, 12].

As the contact overlap has been the dominant contact feature in existing contact models for convex particles, it would be natural to consider developing a generic contact overlap based energy-conserving contact model for all particle shapes, alternative to the contact volume based model [10]. However, there are technical challenges that need to be overcome to achieve this goal within the framework of the energy-conserving contact theory [9].

In our previous work [13], an overlap between two convex polygons/polyhedra is defined based on the Minkowski difference of the two shapes. Then two algorithms, GJK [14] and Expanded Polytope Algorithm (EPA) [15], which are compatible with the overlap defined, are jointly used as the contact detection procedure for convex polygons/polyhedra. Numerical examples indicate that this Minkowski deference based contact modelling procedure is effective and robust. Strong evidence also indicates the proposed contact model is energy-conserving. However, this very desirable property could not be rigorously approved. In addition, there are some practical issues that need to be resolved when computing contact features in some special cases. As this overlap based contact model is specifically developed for convex polygons/polyhedra, a more important question is: can this Minkowski difference based contact overlap be extended to other convex shapes or even to all non-convex shapes?

The main objective of the current work is to positively address the above question, and in particular to extend the previous work [13] in the following aspects. 1) *Conceptually* extend the overlap based on Minkowski difference to be a generic contact overlap definition for both convex and concave shapes, and formally term it as the *Minkowski overlap*; 2) *Theoretically* prove the important property of the Minkowski overlap for convex shapes that leads to an overlap based energy-conserving contact model for convex particles within the general energy-conserving contact theory established in [9]; and 3) *Practically* resolve the uniqueness and ambiguity issues associated with EPA as initially identified in [13]. The present work will serve as the first important step towards the establishment of a unified overlap based energy-conserving contact model for general shaped particles.

As both GJK and EPA used in [13] are for convex polygons/polyhedra, and although they can be extended to convex shapes, they cannot be modified in a simple manner to deal with non-convex shapes. Instead, substantial work is needed to develop new computational procedures for general non-convex cases. For this reason, the current work will mainly focus on convex particles, although any property that is held for both convex and non-convex particles will be mentioned. The new developments of the overlap based energy-conserving contact model for arbitrarily shaped particles will be reported elsewhere.

The paper is organised as follows. The next section will present the definition of the Minkowski overlap between two arbitrarily shaped particles (either convex or concave) in contact, together with the definition of the other related contact features. The derivation of a unique property that the Minkowski overlap exhibits will be provided but limited to convex cases. Both GJK and EPA for convex shaped particles will be briefly outlined in

Section 3 in order to resolve the uniqueness and ambiguity issues associated with the contact features obtained by EPA. A brief discussion is also conduct for extending GJK and EPA to implicitly defined convex particle shapes. Section 4 proposes a Minkowski overlap based energy-conserving contact model for convex particles. The energy-conserving property for cases where the contact normal direction and point may be subject to discrete changes is also rigorously proved. Numerical examples are conducted in Section 5, first to verify the energy-conserving property of the proposed contact model for elastic impact, and then to illustrate the robustness of the whole methodology developed in the current work. Conclusions are drawn in Section 6.

Note that all definitions and computational procedures proposed in this work are applicable to any convex shapes. However for numerical simulations, analytically defined convex shapes, such as super-quadrics, will be discretised into convex polygons/polyhedra first, and then the related contact problem is reduced to the contact of convex polygons/polyhedra which can be effectively handled by the computational procedures outlined in this work.

2 Minkowski Contact Features for Shapes in Contact

Consider two arbitrary geometric shapes (convex or concave), A and B, in 2D or 3D space with boundaries ∂A and ∂B respectively. Their contact state can be classified as

$$\text{Contact State:} \quad \begin{cases} \text{separation} & \equiv & A \cap B = \varnothing \\ \text{touch} & \equiv & A \cap B = \partial A \cap \partial B \\ \text{overlap} & = & A \cap B \neq \varnothing \end{cases}$$

The contact detection phase in DEM is to determine the contact state of the two shapes, and compute some contact features if an actual contact exists. Strictly speaking, this is a pure geometric problem. However, different solution strategies may result in different definitions of contact features and further lead to different mechanical behaviour of particles. It may also significantly affect the computational efficiency involved. More fundamental issues associated with the consistent definition of contact features are covered in [9, 10, 11], where a theoretical framework is provided to decide which features are needed and how they should be defined in consistent with the contact force models used.

The structure of the presentation in this and next sections largely follows two sections in [13] for two reasons: 1) Minkowski difference plays a central role in both the previous work [13] and the current one; and 2) the two core methodologies, GJK and EPA, and their algorithmic implementation still form the backbone for modelling contact between convex particles in general. Thus the main format of describing Minkowski difference, GJK and EPA in [13] is re-attained for completeness and necessity of the further extension in the current work. However, a new concept, namely the *Minkowski overlap* as mentioned in the introduction, will be introduced as a unified definition of contact overlap for all particle shapes, followed by the definition of the related Minkowski contact features for a contact pair. In addition, a very important property of this new overlap definition for convex shapes will be proved which serves as the theoretical foundation for the energy-conversing nature of a Minkowski overlap based contact model to be presented in Section 4.

2.1 Minkowski Sum and Difference of Two Shapes

A geometric shape, either in 2D or 3D, is considered to be the set of all individual points contained in the shape. The Minkowski sum of two shapes A and B defines a new geometric

shape, denoted as $A \oplus B$, by adding every point in A to every point in B:

$$A \oplus B = \{\mathbf{a} + \mathbf{b} : \mathbf{a} \in A, \mathbf{b} \in B\} \tag{1}$$

The Minkowski difference of A and B, denoted as $A \ominus B$, is defined here to be the Minkowski sum of A and $(-B)$:

$$A \ominus B = \{\mathbf{a} - \mathbf{b} : \mathbf{a} \in A, \mathbf{b} \in B\} \tag{2}$$

where $(-B)$ can be viewed as the point reflected image of B in the origin:

$$-B = \{-\mathbf{b} : \mathbf{b} \in B\}$$

The boundary of $A \ominus B$ is denoted as $\partial(A \ominus B)$. It is obvious that only boundaries of A and B will form $\partial(A \ominus B)$, i.e.

$$\partial(A \ominus B) \subset \partial A \ominus \partial B \tag{3}$$

Some basic properties of Minkowski sum and Minkowski difference are stated in [13] and can also be found elsewhere. See for instance in [18, 19] where the term entry block is used instead of the Minkowski difference. The following properties are particularly useful for convex shapes. The Minkowski sums/difference of two convex shapes is also convex, and the Minkowski sum/difference of two convex polygons or polyhedra is a convex polygon or polyhedron.

In addition, the boundary of $A \oplus B$ or $A \ominus B$ is the convex hull of the boundary/vertex sum of A and B or A and $-B$. This property provides an effective approach to explicitly construct the Minkowski sum or difference of two convex polygons/polyhedra if needed. Furthermore, every boundary geometric feature (vertex, edge or face for 3D) of $A \ominus B$ is formed by two boundary features, one from each shape.

For non-convex shapes, the above properties no longer hold. However, when a general shape can be decomposed into convex components, their Minkowski sum or difference can be obtained as the union of all sums or differences of the convex components.

As will be shown below, Minkowski difference is directly relevant to contact modelling of shapes in DEM, while Minkowski sum will no longer be considered.

The algebraic definition of Minkowski difference (2) is rather abstract. A simpler geometric approach can be used to construct the Minkowski difference of two shapes A and B: Fix A and slide B in translation only around A to make sure that A and B are always kept in a touch contact condition. Then the complete trajectory of any point associated with B is the Minkowski difference $A \ominus B$. The drawback of this geometric approach is that the resulting $A \ominus B$ lacks the spatial position which is required for the subsequent contact detection using the origin in the point inclusion test as described below.

Figure 1 illustrates the Minkowski differences of a fixed quadrilateral (A) with an ellipse (B) at three different vertical positions, where the Minkowski difference $A \ominus B$ remains the same but its spatial position shifts vertically.

2.2 Minkowski difference and Contact State

When A and B are in contact (in touch or overlap/penetration), there must exist at least one point $\mathbf{p}$ that is located in the two shapes: $\mathbf{p} \in A; \mathbf{p} \in B$. By the definition (2), the corresponding Minkowski different point of these two pints must be the origin $\mathbf{o}$. In other

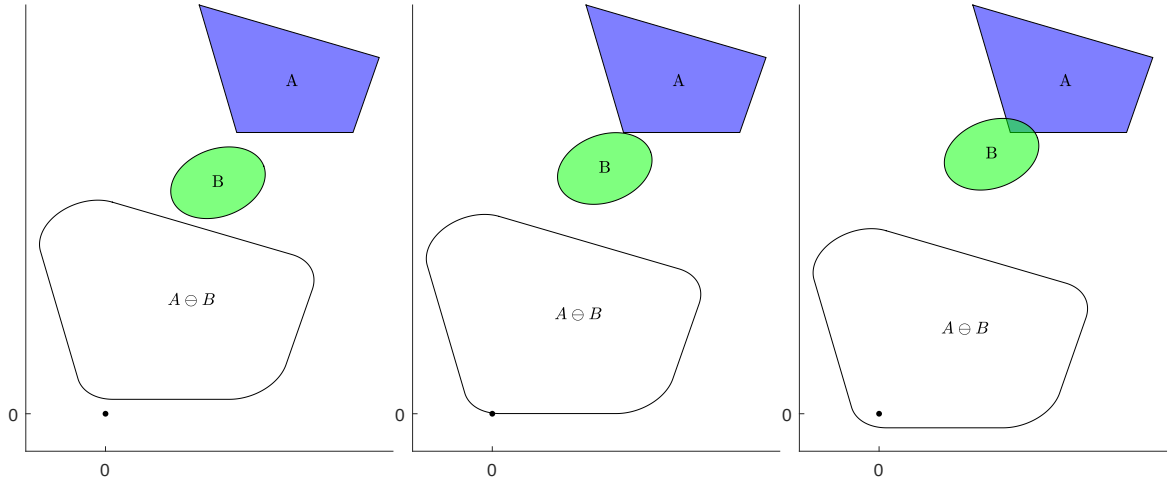

(a) Separation (b) Touch (c) Overlap

Figure 1: The Minkowski difference of a fixed quadrilateral A with an ellipse B at three different vertical positions corresponding to three contact states

words, if A and B are in contact, the origin must be enclosed in the Minkowski difference $A \ominus B$, and vice versa:

$$\mathbf{o} \in A \ominus B \iff A \cap B \neq \varnothing \tag{4}$$

Consequently, the contact state of two shapes A and B is equivalent to determining if $\mathbf{o}$ belongs to $A \ominus B$ or not, which is a point inclusion test. However, the point inclusive test requires the explicit construction of the Minkowski difference which may not be straightforward and could be computationally expensive. Thus, the Minkowski difference provides a conceptually simple and universal approach to determining the contact state of any two shapes, but its effectiveness will largely depend on how effective the point inclusion test will be conducted.

The three figures in Figure 1 clearly demonstrate that the relationship between the Minkowski difference and the origin is equivalent to the contact state of the two shapes. When B moves in translation only, the shape and orientation of the Minkowski difference remain unchanged, but its spatial position moves in the opposite direction.

2.3 Minkowski Difference Distance and Overlap

The translation of shape A by a (vector) distance $\mathbf{v}$ that is also considered to be the sole element of a set $\{\mathbf{v}\}$, can be defined using Minkowski sum as

$$A^{\mathbf{v}} \equiv A \oplus \{\mathbf{v}\} = \{\mathbf{a} + \mathbf{v} : \mathbf{a} \in A\} \tag{5}$$

Then the Minkowski difference of the $\mathbf{v}$-translated A and B is

$$A^{\mathbf{v}} \ominus B = \{\mathbf{a} + \mathbf{v} - \mathbf{b} : \mathbf{a} \in A, \mathbf{b} \in B\} = (A \ominus B) \oplus \{\mathbf{v}\} = (A \ominus B)^{\mathbf{v}} \tag{6}$$

Similarly we have the Minkowski difference of A with the $\mathbf{v}$-translated B as

$$A \ominus B^{\mathbf{v}} = \{\mathbf{a} - (\mathbf{b} + \mathbf{v}) : \mathbf{a} \in A, \mathbf{b} \in B\} = (A \ominus B) \oplus \{-\mathbf{v}\} = (A \ominus B)^{-\mathbf{v}} \tag{7}$$

Thus, applying a translation to A is equivalent to having the same translation to $A \ominus B$; while the translation of B causes an opposite translation to $A \ominus B$.

The *vector distance* between A and B, denoted as $\mathbf{d}_M$, is defined as the minimum translational distance $\mathbf{v}$ required to be applied to B such that A and $B^{\mathbf{v}}$ are just in touch

$$\mathbf{d}_M = \underset{\mathbf{v}\in\mathbb{R}^n}{\operatorname{argmin}}\{\|\mathbf{v}\| : \mathbf{o} \in \partial(A \ominus B^{\mathbf{v}})\} \tag{8}$$

Alternatively, $\mathbf{d}_M$ is also the minimum vector distance from the origin $\mathbf{o}$ to the boundary of $A \ominus B$:

$$\mathbf{d}_M = \underset{\mathbf{v}\in\mathbb{R}^n}{\operatorname{argmin}}\{\|\mathbf{v}\| : \mathbf{v} \in \partial(A \ominus B)\} \tag{9}$$

Express the vector distance $\mathbf{d}_M$ as

$$\mathbf{d}_M = \delta_M \mathbf{n}_M \tag{10}$$

where $\delta_M = \|\mathbf{d}_M\|$ is the scalar distance which is normally called the gap when the shapes are in separation, or the overlap when they are in penetration; and $\mathbf{n}_M$ is a unit vector.

Now, $\mathbf{d}_M$ is termed the *vector Minkowski-difference distance*, or the *vector Minkowski distance* for short, while δ_M is termed the *scalar Minkowski difference-distance*, or the *Minkowski overlap* for short. The direction $\mathbf{n}_M$ is termed as the *(Minkowski) contact normal*. For simplicity, the term *Minkowski overlap* will be used for both vector and scaler Minkowski-difference distances.

It is emphasised that the above definition of the vector or scalar Minkowski difference distance is applicable to both convex and concave shapes with either flat or curved boundaries. In fact, the Minkowski overlap recovers the conventional overlap used for discs and spheres and is also equivalent to the overlap established using the common-normal concept for smooth non-spherical particles [6]. The significance of this definition is that it also covers shapes with sharp edges and vertices such as cylinders and polygons/polyhedra, and therefore it provides a generic definition of contact overlap for any shapes involved. More importantly, the Minkowski overlap possesses a unique property, as will be derived in the next subsection, which is crucial to the establishment of an overlap based energy-conserving contact model to be introduced in Section 4.

However, the discussion below will be restricted to convex shapes, and the relevant theoretical and numerical issues for concave shapes will be addressed elsewhere.

2.4 Geometric Properties of Minkowski Overlap: Contact Features

2.4.1 Minkowski contact features

Refer to Figure 2 for the contact between two (convex) shapes A and B with B at two slightly different positions. The shortest distance, or Minkowski distance, is the vector from the origin $\mathbf{o}$ to its orthogonal projection on the boundary of $A \ominus B$, $\partial(A \ominus B)$, and is denoted as $\mathbf{c}$ and is called the contact point on $A \ominus B$. The two corresponding contact points associated with $\mathbf{c}$ on the boundaries of A and B are respectively $\mathbf{c}_1$ and $\mathbf{c}_2$. By the definition of the Minkowski distance (9), we have

$$\mathbf{d}_M = \delta_M \mathbf{n} = \mathbf{c} - \mathbf{o} = \mathbf{c}_1 - \mathbf{c}_2 \tag{11}$$

with $\mathbf{n}_M = \mathbf{c}/\|\mathbf{c}\| = (\mathbf{c}_1 - \mathbf{c}_2)/\|\mathbf{c}_1 - \mathbf{c}_2\|$, $\delta_M = \|\mathbf{c}\| = \|\mathbf{c}_1 - \mathbf{c}_2\|$. Obviously, $\mathbf{n}_M$ is the normal of $\partial(A \ominus B)$ at $\mathbf{c}$. Furthermore, both $\mathbf{n}_M$ and the overlap distance vector $\mathbf{c}_1\mathbf{c}_2$ are the common normal to both A and B if $\mathbf{c}_1$ and $\mathbf{c}_2$ are not vertices.

In Figure 2(a), $\mathbf{c}_1$ is a vertex of A, while $\mathbf{c}_2$ is on the boundary/edge of B so the line $\mathbf{c}_1\mathbf{c}_2$ is the normal of B at $\mathbf{c}_2$. Following the classification of different contact types in [13], this

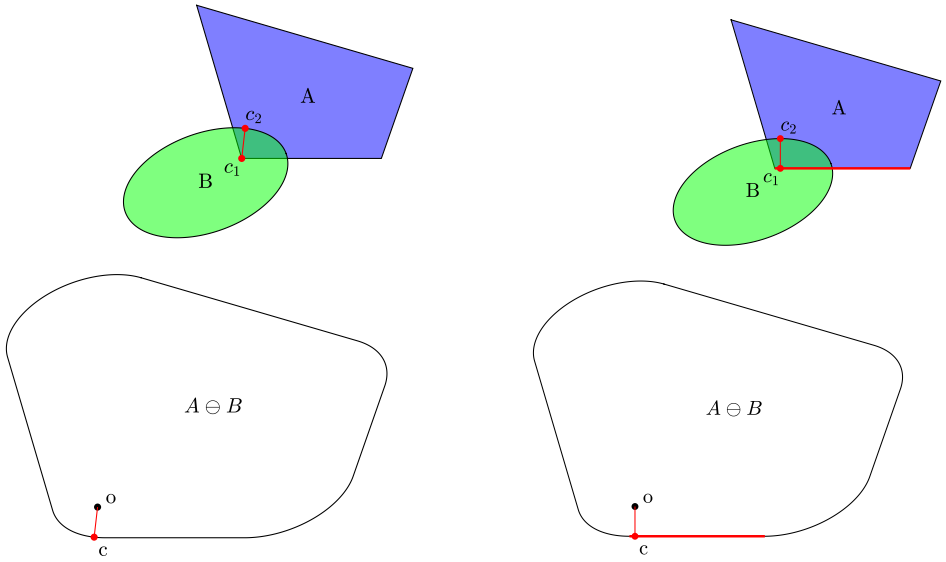

(a) Vertex-Edge (b) Edge-Edge

Figure 2: The contact features and types between A and B in two cases: contact point $\mathbf{c}$ on $A \ominus B$, contact points $\mathbf{c}_1$ and $\mathbf{c}_2$ on A and B respectively; $\mathbf{oc}$ defines the contact normal $\mathbf{n}$ and is perpendicular to $\partial(A \ominus B)$; while $\mathbf{c}_1\mathbf{c}_2$ is the normal of B at point $\mathbf{c}_2$ in (a) and (b), and also normal to the bottom edge of A in (b)

contact can be classified as a "vertex-edge" contact. While in Figure 2(b), $\mathbf{c}_1$ is a point on the edge of A. So $\mathbf{c}_1\mathbf{c}_2$ is a common normal to both A and B, and the contact type is "edge-edge". In a contact model, a common contact point $\mathbf{c}_M$ for both A and B needs to be specified. One reasonable option is to set $\mathbf{c}_M$ to be the middle point of $\mathbf{c}_1$ and $\mathbf{c}_2$:

$$\mathbf{c}_M = (\mathbf{c}_1 + \mathbf{c}_2)/2 \tag{12}$$

There is a theoretical justification [16] for such a choice if A and B have the same elastic material properties and the contact does not involve sharp corners and edges. In what follows, $\mathbf{d}_M, \delta_M, \mathbf{n}, \mathbf{c}, \mathbf{c}_1, \mathbf{c}_2$ and $\mathbf{c}_M$ are all collectively called the *Minkowski contact features*.

2.4.2 Gradient of the Minkowski overlap

Now consider shape B that is subject to a translational motion and choose the coordinates of an arbitrary reference point as $\mathbf{x}$. Then $\mathbf{c}, \mathbf{c}_1, \mathbf{c}_2, \mathbf{d}_M, \delta_M$ and $\mathbf{n}_M$ are all functions of $\mathbf{x}$. Below will derive the gradient of δ_M with respect to $\mathbf{x}$.

Since $\mathbf{n}_M \cdot \mathbf{n}_M = 1$, it has

$$\mathbf{n}_M \cdot \frac{\partial \mathbf{n}_M}{\partial \mathbf{x}} = 0 \tag{13}$$

or

$$\mathbf{c} \cdot \frac{\partial \mathbf{n}_M}{\partial \mathbf{x}} = \delta_M \mathbf{n}_M \cdot \frac{\partial \mathbf{n}_M}{\partial \mathbf{x}} = 0 \tag{14}$$

Rewrite δ_M as

$$\delta_M = \mathbf{c} \cdot \mathbf{n}_M \tag{15}$$

Then

$$\frac{\partial \delta_M}{\partial \mathbf{x}} = \frac{\partial \mathbf{c}}{\partial \mathbf{x}} \cdot \mathbf{n}_M + \mathbf{c} \cdot \frac{\partial \mathbf{n}_M}{\partial \mathbf{x}} \tag{16}$$

Utilising (14) gives

$$\frac{\partial \delta_M}{\partial \mathbf{x}} = \frac{\partial \mathbf{c}}{\partial \mathbf{x}} \cdot \mathbf{n}_M \tag{17}$$

As δ_M is the shortest distance between $\mathbf{o}$ and $\partial(A \ominus B)$, it has

$$\frac{\partial \mathbf{c}}{\partial \mathbf{x}} = -\mathbf{I} \quad \text{(identity matrix)} \tag{18}$$

which leads to

$$\frac{\partial \delta_M}{\partial \mathbf{x}} = -\mathbf{n}_M \tag{19}$$

This is the most important property of the proposed Minkowski overlap and it ensures that the contact model presented in Section 4 will be energy conserving. It also has a clear geometric explanation that the most effective way to move B to reduce the overlap δ_M must be along the negative direction of the contact normal $\mathbf{n}_M$. It should be highlighted that this property (19) is held for both convex and concave shapes, but only convex shapes will be considered in the next section.

As a final note, the (scalar) Minkowski distance δ_M defined above is equivalent to the (positive) signed distance of the origin to the boundary of $A \ominus B$, $\partial(A \ominus B)$, and thus should satisfy the so called Eikonal equation

$$\left|\frac{\partial \delta_M}{\partial \mathbf{x}}\right| = 1 \tag{20}$$

where the origin is conceptionally treated as a moving point relative to the now stationary $\partial(A \ominus B)$. Clearly the derived property (19) indeed satisfies this Eikonal equation.

3 Minkowski-difference Based Contact Detection Procedures

The computational procedures associated with obtaining the Minkowski overlap/distance of two convex shapes will be discussed in this section, including the definition of a support point for a shape; the GJK algorithm for detecting if two shapes are in contact or not, and the evaluation of the Minkowski contact features using EPA. Also, the solutions to the two previously unresolved issues in [13] are also presented.

3.1 Support Point of Shapes

For a given vector $\mathbf{v} \neq 0$ as the search direction, the *support point (or function)* of shape A along $\mathbf{v}$, denoted as $\mathbf{p}_s(A, \mathbf{v})$, is defined by

$$\mathbf{p}_s(A, \mathbf{v}) = \mathbf{p} \in A : \ \mathbf{p} \cdot \mathbf{v} \geqslant \mathbf{q} \cdot \mathbf{v}, \ \forall \mathbf{q} \in A \tag{21}$$

which is the furthest point of A along the direction $\mathbf{v}$. Since $\mathbf{q} \cdot \mathbf{v}$ can be viewed as the (projected) coordinate of the point $\mathbf{q}$ in the direction $\mathbf{v}$, the support point $\mathbf{p}_s$ is thus the point in A that has the maximum projected coordinate along the direction.

The support point for $-A$, which is the reflected shape of A in the origin, can be obtained by the definition (21) as:

$$\mathbf{p}_s(-A, \mathbf{v}) = -\mathbf{p}_s(A, -\mathbf{v}) \tag{22}$$

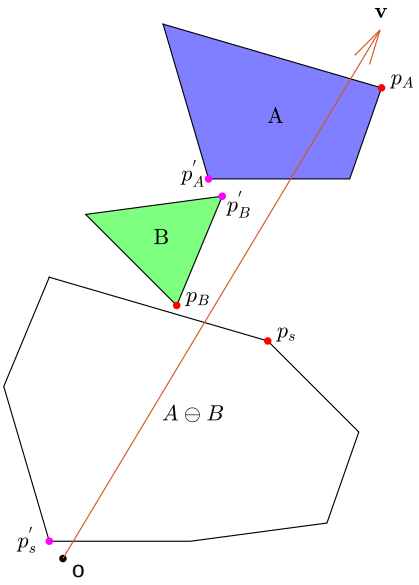

Figure 3: The support points of A, B and $A \ominus B$ along search directions $\mathbf{v}$: p_A, p_B and p_s, and also their support points p'_A, p'_B and p'_s along $-\mathbf{v}$

i.e. the furtherest point of $-A$ along the search direction is the origin reflection of the support point of A along the opposite direction of $\mathbf{v}$. Thus the support point for the Minkowski difference of A and B can be expressed as:

$$\mathbf{p}_s(A \ominus B, \mathbf{v}) = \mathbf{p}_s(A, \mathbf{v}) + \mathbf{p}_s(-B, \mathbf{v}) = \mathbf{p}_s(A, \mathbf{v}) - \mathbf{p}_s(B, -\mathbf{v}) \tag{23}$$

This expression is significant in the sense that there is no need to explicitly construct $A \ominus B$ in order to compute its support point. In other words, as long as the support points for A and B can be defined, the support point for $A \ominus B$ can be readily obtained from the support points of A and B. This entirely avoids the often very costly explicit generation of $A \ominus B$. It also benefits greatly for complex shapes that are implicitly defined such as by the Minkowski sum of a number of (simpler) constituent shapes where their individual support functions are defined. Figure 3 illustrates the support points of a quadrilateral, a triangle and their Minkowski difference for two search directions $\mathbf{v}$ and $-\mathbf{v}$.

Some properties of the support point of the Minkowski difference $A \ominus B$ are stated in [13]. The following one is very important: A and B are not in contact if there exists a search direction $\mathbf{v}$ such that

$$\mathbf{v} \cdot \mathbf{p}_s(A \ominus B, \mathbf{v}) = \mathbf{v} \cdot \mathbf{p}_s(A, \mathbf{v}) - \mathbf{v} \cdot \mathbf{p}_s(B, -\mathbf{v}) < 0 \tag{24}$$

This property can be geometrically interpolated in two different ways. Firstly, the direction $\mathbf{v}$, together with the origin $\mathbf{o}$, can define a one-dimensional coordinate system. The left hand side $\mathbf{v} \cdot \mathbf{p}_s(A \ominus B, \mathbf{v})$ is the maximum projected coordinate of the shape $A \ominus B$ on $\mathbf{v}$. Then if this maximum coordinate is negative, the origin, which has the zero projected coordinate on $\mathbf{v}$, is further than any point in $\partial(A \ominus B)$ along the direction $\mathbf{v}$, and thus the origin must be outside of $A \ominus B$, i.e. A and B are not in contact.

Alternatively, $\mathbf{v} \cdot \mathbf{p}_s(A, \mathbf{v})$ can be regarded as the maximum projection or local coordinate of A along $\mathbf{v}$; while $\mathbf{v} \cdot \mathbf{p}_s(B, -\mathbf{v})$ can be regarded as the minimum projection or local coordinate of B along $\mathbf{v}$. (24) states that if the maximum projection of A is smaller than the minimum projection of B on the direction $\mathbf{v}$, then both shapes must not be in overlap. In Figure 3, the

origin $\mathbf{o}$ is further in the search direction $-\mathbf{v}$ than the support point $\mathbf{p}'s$ of the Minkowski difference $A \ominus B$, so A and B must not be in contact.

The support point of a shape along a particular direction may not be unique. For instance, any point on a straight edge or on a flat face can be the support point when the whole edge or face is the furtherest along a direction that is perpendicular to the edge or face. The implication of this fact is that an ambiguity issue may arise as pointed out in [13]. How to resolve this issue will be discussed in Section 3.5.

The support point plays an utmost role in both GJK and EPA to be outlined in the next two subsections for contact detection between two convex shapes.

For convex polygons/polyhedra, their support points can be obtained from the vertices alone, and no other topological properties, such as edges and faces, are needed. This feature makes the implementation of the support point computation for polygons/polyhedra straightforward. The complexity of computing one support point is proportional to the sum of the numbers of vertices of the two shapes concerned. More effective algorithms are available for polygons/polyhedra with many vertices, see for instance in [20].

For non-spherical convex shapes, an explicit expression of the support point exists for the following primary geometric entities: ellipses/ellipsoids, simple 2D super-quadrics, cylinders and hemisphere capped cylinders. For other non-spherical convex shapes, in order to define a function to compute a support point without involving nonlinear equation solving, a universal approach is to approximately represent such a shape using a surface triangular mesh so the shape is converted into a convex polyhedron.

3.2 The GJK Algorithm for Obtaining Contact States Between Convex Shapes

For two shapes A and B, the GJK algorithm iteratively searches for a simplex (triangle in 2D and tetrahedron in 3D) with points on the boundary or vertices of $\partial(A \ominus B)$ that contains the origin, or detect a non-contact case when the condition (24) is met for a search direction. The algorithmic detail of GJK can be found in [14] and is also outlined in Appendix A.

The GJK algorithm is one of the most elegant numerical procedures for contact detection, and is applicable to any convex shape as long as the support point can be numerically defined to compute the furthest boundary point along a given research direction. Thus the GJK algorithm offers greater versatility than other similar approaches.

3.3 Expanding Polytope Algorithm for Computing Contact Features

The original GJK algorithm proposed in [14] was intended not only to determine whether the two convex shapes are in contact or not, but also to provide further geometric features of the contact required. However, GJK now is mainly used for the first purpose and other algorithms are developed for computing the contact features of a contact situation. The most popular algorithm to fulfil this task is EPA [15]. Its algorithmic aspect is also described in detail in [13], and outlined in Appendix B.

The main idea of the EPA is to iteratively construct an inscribed polytope $\mathbf{P}$ to the Minkowski difference so that the shortest distance of the origin to one of the flat faces of the polytope is taken as the contact overlap. EPA starts with the simplex outputted from GJK as the initial polytope $\mathbf{P}$. The face closest to the origin in $\mathbf{P}$ is found and its outward normal is used as the next search direction to compute a new support point $\mathbf{a}$ on $\partial(A \ominus B)$. Use this

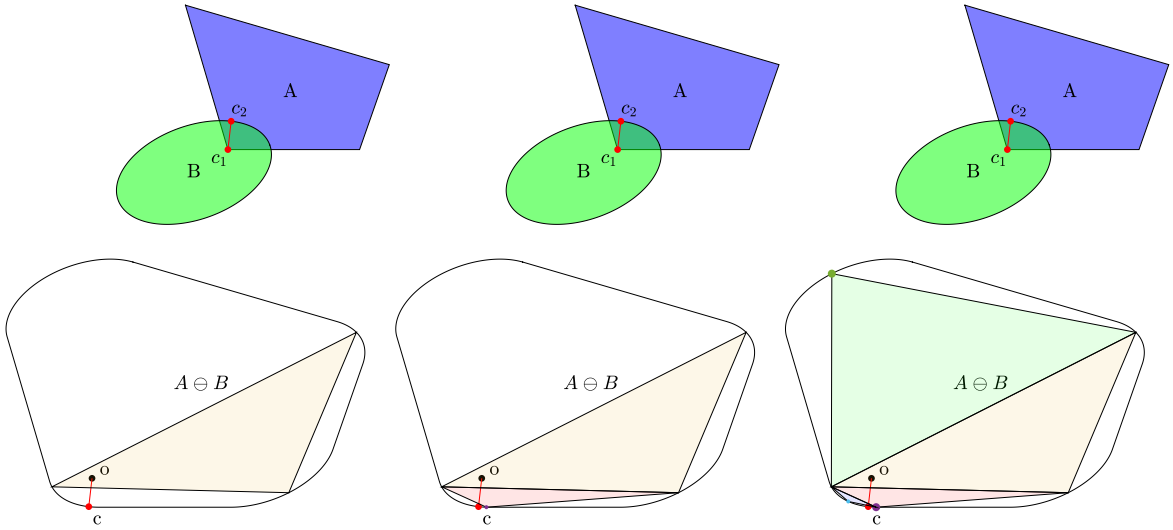

(a) GJK: Output Simplex (b) EPA: 1st iteration (c) EPA: 3rd iteration

Figure 4: EPA iterations: (A) the initial simplex obtained from GJK; (b) the expanded polytope after one EPA iteration; and (c) the expanded polytope after three EPA iterations

new point to update or expand $\mathbf{P}$ by removing some old faces based on their visibility from $\mathbf{a}$ and adding some new faces. Then check if the new shortest distance computed after the new faces added has converged or not. This procedure repeats until the face closest to the origin is also a face of $\partial(A \ominus B)$ for (convex) polygon/polyhedron cases, or the shortest distance converges within a prescribed tolerance for general convex shapes.

Figure 4 illustrates this iteration process for a quadrilateral-ellipse contact pair, where Figure 4(a) displays the simplex (a triangle) from the output of GJK as the initial polytope; while Figure 4(b) and (c) depict the expanded polytope after the first and third iteration respectively. Each EPA iteration adds one new vertices, and two edges and also removes one edge in 2D cases; while the number of removed and added faces in 3D cases is not fixed.

Note that the shortest distance of the origin to the faces of $\mathbf{P}$ provides a lower bound of the true overlap, while the shortest distance between the origin and the vertices of the polytope is an upper bound of the overlap. During the iteration the difference of these two bounds is constantly reducing until the convergence condition is met.

For polygon/polyhedron cases, the shortest distance will be obtained in a finite number of iterations when the new point found is one of the vertices on the face, i.e. the closest face of the polytope is also a face of $\partial(A \ominus B)$. For general convex shapes, the new point may never be an existing vertex of $\mathbf{P}$, so a pre-defined tolerance ϵ has to be introduced to control the termination of the iteration.

When the iteration is terminated, the closest face on $\mathbf{P}$ to the origin $\mathbf{o}$ is determined together with the (approximate) shortest distance which is the Minkowski overlap $\delta_{_M}$. Then the other contact features can be obtained, including contact point $\mathbf{c}$, contact normal $\mathbf{n}_{_M}$, contact point pair $\mathbf{c}_k (k = 1, 2)$ on the two shapes, and contact type if required. The detail can be found in [13].

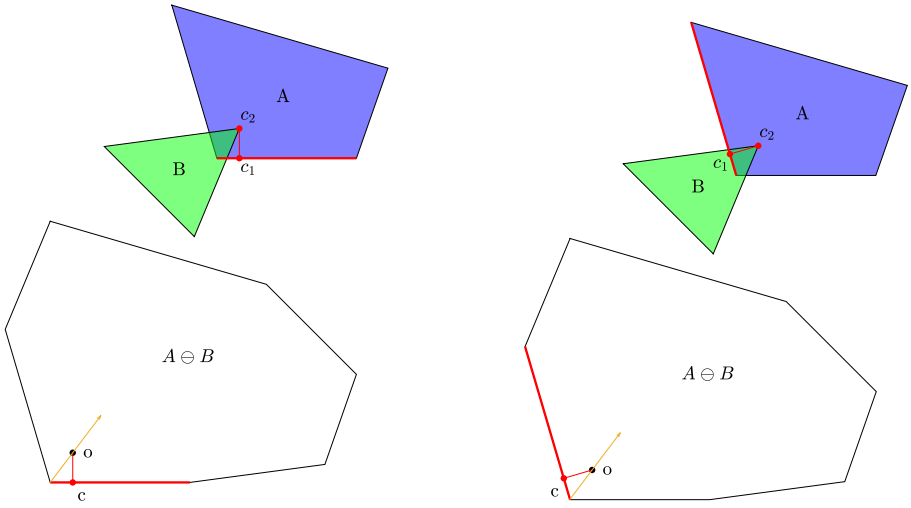

(a) Contact 1 (b) Contact 2

Figure 5: Shapes A and B have two possible contacts with the same Minkowski overlap but distinct contact normals and contact points

3.4 Uniqueness Issue

As discussed in [13], there exist uniqueness and ambiguity issues in some special cases. A uniqueness issue arises when the contact point $\mathbf{c}$ or normal $\mathbf{n}_M$ is not unique, while an ambiguity situation occurs when the contact points $\mathbf{c}_1$ and/or $\mathbf{c}_2$ may have multiple values.

More specifically, a uniqueness issue occurs when the origin has an equal (shortest) distance to multiple points on $\partial(A \ominus B)$, giving rise to possible multiple contact points and directions. This issue is demonstrated in Figure 5 where the origin has the equal distance to two sides of $\partial(A \ominus B)$ which is a polygon. The two possible contact scenarios with two distinct sets of contact features are shown in Figure 5 (a) and (b) respectively.

In theory, these two cases are equally valid, but in practice, only one case will be selected depending (randomly) on numerical round-off errors and also on algorithmic implementation details. The main concern with this uniqueness issue in [13] was that during a DEM simulation, the contact of two shapes in two consecutive time steps may be subject to a *sudden change* from one contact case to the other. As the contact normals and points of these two cases are distinct, and the corresponding contact forces/moments acting on the two shapes can be very different, thus superficial energy could be introduced between these two steps, thereby having potential to cause a numerical instability problem.

However, numerical simulations conducted so far, including those in [13, 23] and also in Section 5, have shown no evidence that such an instability problem occurs. The fundamental reason that no instability will happen due to the sudden change of contact directions and points is theoretically proved in the next section 4. So overall, by defining the contact overlap as the Minkowski overlap, together with the use of the contact model described in the next section, the contact is guaranteed to be energy-conserving and thus no instability will occur. Only issue here is on numerical solution accuracy which is related to the time step used. To achieve a higher numerical accuracy, a smaller time step may be expected to use.

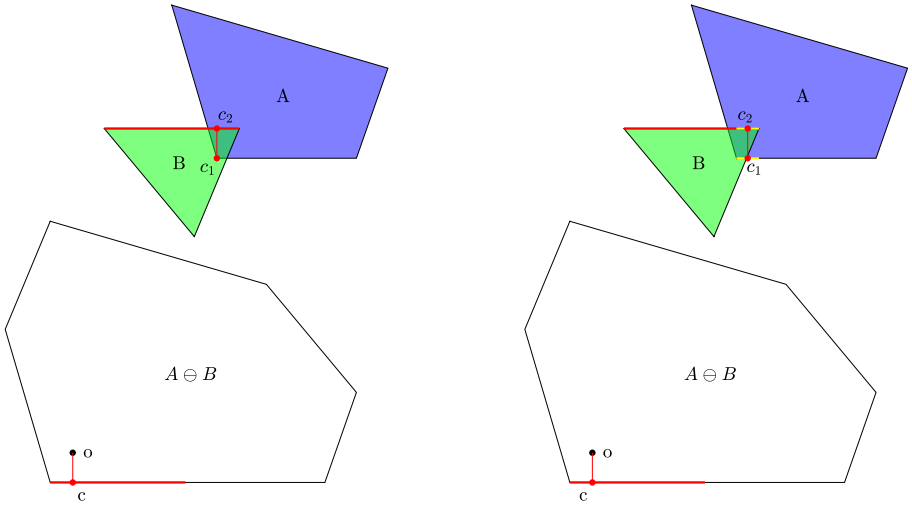

(a) Ambiguity: Edge-edge (b) Solution: Edge-edge

Figure 6: An ambiguous edge-edge contact (a); and the solution (b) with correct contact points

3.5 Ambiguity Issue

The ambiguity issue that was raised in [13] is the ambiguous determination of contact normals and points in some special cases. Such an ambiguous case is depicted in Figure 6(a) where the contact point **c** is unique, and so is the contact normal **n**, but the corresponding contact points on A and B are not unique. Although the figure shows an edge-vertex contact type, the actual contact should be the edge-edge contact between the bottom side of A and the top side of B. Or more precisely the correct contact should be between the projected overlap segments of the two sides, as shown by the yellow segments in Figure 6(b). Then the corresponding contact points should each be the centroid of the projected overlap segment on each shape. This pair of contact points are marked in Figure 6(b). Similar procedures can be applied to edge-edge/face or face-face contacts for polyhedra or shapes with straight edges and/or flat faces. Again, the key to resolving the ambiguity issue is to ensure that the contact points on A and B should be the centroids of the projected contact area from each shape. Thus by correctly determining the two contact points for these special cases, the ambiguity issue is now fully resolved.

3.6 Combined Solution Strategy to Curved Shapes

As same as GJK, EPA can also be applied to any convex shapes in principle. Since the nature of EPA is to use a polytope to (partially) approximate the $A \ominus B$, this approach works very efficiently for convex polygons/polyhedra. However the algorithm is not effective for convex shapes with curved boundaries, due to the slow convergent rate of the polytope approximation to a curved $A \ominus B$, as numerically showed in [13].

For a pair of curved shapes, their Minkowski overlap is the orthogonal distance between the two shapes which is equivalent to (9). Traditionally, this distance can be found by simultaneously solving a set of nonlinear equations associated with the shapes. However, the solution often suffers from poor convergence or total failure mainly due to poor initial guesses.

A better solution to the case with curved shapes is to combine EPA with traditional nonlinear equation solving approaches. In this two-step hybrid approach, EPA is used first to compute the contact points of the shapes with a fairly large convergent tolerance ϵ. Or if a high accuracy is not required in this step, the shapes could also be approximated as polygons/polyhedra with fairly coarse surface meshes. Then the computed contact points on the two shapes from EPA can now be employed as the initial guess for the solution of the nonlinear equations concerned in the second step. An optimal solution with the least computational cost could be achieved for a pair of particular shapes by tuning some parameters used in this two-step approach. No detailed investigation of this issue will be presented in the current work.

4 Contact Overlap Based Energy-Conserving Contact Model

After all the contact geometric features of two contacting particles are found, the goal of a normal contact model is to compute the normal contact forces in terms of these contact geometric features. Such a normal contact model will be proposed within the framework of an energy-conserving contact theory rigorously established in [9] where the contact is fully characterised by a contact energy function or potential w.

Consider w to a function of the Minkowski overlap $\delta_{_M}$. As the overlap is independent of the global coordinate system, any monotonically increasing function of the overlap clearly satisfies both translational and rotational invariances required for the function w [9], and therefore can be a valid candidate as the contact energy function. As a result, alternative to the contact volume based contact models presented in [10], a generic Minkowski overlap based normal contact model is proposed below.

[Minkowski Overlap Based Normal Contact Model] *Let* $\mathbf{d} = \delta_{_M}\mathbf{n}_{_M}$ *be the vector Minkowski distance of two bodies in contact, where* $\delta_{_M}$ *is the scalar distance or overlap and* $\mathbf{n}_{_M}$ *is the unit normal direction of the contact. Also* $\mathbf{c}_{_M}$ *is the (Minkowski) contact point. Let* $w(\delta_{_M})$ *be a monotonically increasing function of the contact overlap* $\delta_{_M}$*. Then the elastic energy of the contact will be conserved if the normal force* $\mathbf{F}_n$ *exerted on body 1 by body 2 can be obtained as*

$$\mathbf{F}_n = -\nabla_x w(\delta_{_M}) = F_n\,\mathbf{n}_{_M} \tag{25}$$

where the magnitude of the force $F_n = dw(\delta_{_M})/d\delta_{_M} \equiv w'(\delta_{_M})$*. The normal force* $\mathbf{F}_n^*$ *exerted on body 2 by body 1 is*

$$\mathbf{F}_n^* = -\mathbf{F}_n = -F_n\mathbf{n}_{_M} \tag{26}$$

Both forces act at the common contact point $\mathbf{c}_{_M}$ *on the two bodies separately.*

Following the theoretical framework developed in [9], the key to the above Minkowski overlap based contact model with an energy-conserving nature is the requirement of the following relationship to be held

$$\nabla_{\mathbf{x}}\delta_{_M} = \frac{\partial\delta_{_M}}{\partial\mathbf{x}} = -\mathbf{n}_{_M} \tag{27}$$

where $\mathbf{x}$ is taken to be the coordinates of a reference point on body 2. This relationship is exactly the property of the Minkowski overlap that is established in (19), and thus the above Minkowski overlap based contact model must be energy-conserving.

Nevertheless, as demonstrated in Section 3.4, both the normal force direction $\mathbf{n}_{_M}$ and contact point $\mathbf{c}_{_M}$ can be subject to a sudden or discrete change (but the overlap remains to

be continuous) under a small movement. Therefore a natural question arises: would such a discrete change of contact force direction and position violate the energy-conserving property claimed above and subsequently causes numerical instability? This issue is rigorously addressed below.

First of all, the definition of the normal force $\mathbf{F}_n$ by (25) is equivalent to the fact that the contact energy $w(\delta_M)$ is the so called anti-derivative of $\mathbf{F}_n$ [17]. Then, following the theoretical development in [9], the work done by resisting the contact force $\mathbf{F}_n$ acting on body 1 over an arbitrary path $\mathcal{L}_{\mathbf{a}\to\mathbf{b}}$ from a point $\mathbf{a}$ to a point $\mathbf{b}$ in the configuration space can be expressed as

$$W(\mathcal{L}_{\mathbf{a}\to\mathbf{b}}) = -\int_{\mathcal{L}_{\mathbf{a}\to\mathbf{b}}} \mathbf{F}_n \cdot d\mathbf{x} + \left((\bar{\mathbf{x}} - \mathbf{c}_M) \times \mathbf{F}_n\right) \cdot d\boldsymbol{\theta} \tag{28}$$

where $\bar{\mathbf{x}}$ is the mass centre of body 1. A sudden change of $\mathbf{n}_M$ and $\mathbf{c}_M$ corresponds to a discontinuous point of $\mathbf{F}_n$ as a function over the path. Clearly, the total number of such discontinuous points along the path will be limited, or their *Lebesgue measure* is zero, and therefore the above integral is Riemann integrable [17]. Consequently, by virtue of the second fundamental theorem of calculus [17] or the Newton-Leibniz axiom, together with the fact that $w(\delta_M)$ is the anti-derivative of $\mathbf{F}_n$, it has

$$W(\mathcal{L}_{\mathbf{a}\to\mathbf{b}}) = w(\delta_{M|\mathbf{b}}) - w(\delta_{M|\mathbf{a}}) \tag{29}$$

where $\delta_{M|\mathbf{a}}$ and $\delta_{M|\mathbf{b}}$ are the Minkowski overlaps at the points $\mathbf{a}$ and $\mathbf{b}$ respectively. This expression states that the total work done from $\mathbf{a}$ to $\mathbf{b}$ is path independent, which as discussed in [9], leads to the conclusion that the energy-conserving property of the Minkowski overlap based normal contact model proposed above is theoretically ensured, even if the contact force direction and contact point may undergo some discontinuous jumps.

Thus, the above Minkowski overlap based contact model, together with the procedures to obtain the Minkowski contact features discussed in the previous section, fully describes all the aspects of a normal contact force: normal direction, magnitude and contact point, and guarantees elastic energy conservation in any contact scenario and thereby ensuring robust and stable discrete element simulations for complex problems.

The above contact model is generic in the sense that many different forms of the contact energy potential or function $w(\delta_M)$ can be specified as along as they are monotonically increasing. For instance, $w(\delta_M)$ can be chosen as a general power-law function of the overlap

$$w(\delta_M) = \frac{1}{n+1} k_n \delta_M^{n+1} \tag{30}$$

where k_n is the (nominal) stiffness and $n \geqslant 1$. The corresponding force magnitude has the form

$$F_n = k_n \delta_M^n \tag{31}$$

from which both classic linear $(n = 1)$ and Hertz-type $(n = 3/2)$ models can be recovered.

Note that for two circular discs or spheres, the Minkowski overlap reduces to the standard overlap for such shapes, and thus the proposed contact model reduces to the linear or Hertz contact model when the exponent n is set to be 1 or 3/2, provided that a proper normal stiffness k_n can also be set. Clearly, these standard contact models for discs/spheres are energy-conserving, i.e. the existing overlap based disc/sphere contact models are special cases of the current Minkowski overlap based contact model.

It is emphasised that although the force magnitude expression (31) is nothing new, the fundamental difference of the proposed model from conventional overlap based models is how the

overlap is defined for non-spherical particles. The current development theoretically proves that when the overlap is defined as the Minkowski distance equipped with the Minkowski contact normal and point, the elastic potential energy-conserving property can be achieved. Otherwise, energy will not be conserved in all cases, leading to potential numerical instability issues in some complicated situations.

Finally, the proposed contact model is equally applicable to general concave cases, where the property (19) is also held. The major challenge is how to obtain all the Minkowski features correctly and effectively for a pair of concave shapes where both GJK and EPA for convex particles are no longer applicable in most cases. The related developments to effectively obtain the Minkowski contact features for general non-convex particles are substantial and will be reported elsewhere.

5 Numerical Examples

Two sets of examples, each with two numerical cases, are presented in this section. In the first two examples each involves three particles in elastic impact with the aim to verify the energy-conserving property of the Minkowski overlap based contact model. The other two examples, consisting of a (relatively) large number of particles with different shapes, attempt to demonstrate the robustness of the proposed methodologies. No attempt is made to compare the numerical efficiency of the current methodology with, for instance, the contact volume based contact model [10] which is equally applicable here and also conserves elastic energy. The efficiency investigation will be done elsewhere.

The classic central difference scheme is employed as the time integrator to solve the translational motion of the particles, while the rotational motion is resolved by a symplectic time integration scheme [22] in conjunction with the quaternion representation of the particle orientation. The algorithm is also presented in [23].

5.1 Energy Conservation Verification

Verification 1: Elastic impact of three super-quadrics.

This example consists of three super-quadric particles, with their surfaces analytically expressed as [21]

$$\left(\left|\frac{x}{a}\right|^{n_2} + \left|\frac{y}{b}\right|^{n_2}\right)^{n_1/n_2} + \left|\frac{z}{c}\right|^{n_1} - 1 = 0 \tag{32}$$

but with different constants a, b, c, n_1 and n_2. Refer to Figure 7(a), which shows the initial configuration of the three particles, the constants used to define these three particles are as follows: the top particle: $a = 1.5, b = 0.4, c = 3, n_1 = 3, n_2 = 10$; the middle one: $a = 2, b = 1, c = 1, n_1 = 2, n_2 = 10$, and the bottom particle: $a = 2, b = 1, c = 1.5, n_1 = 3, n_2 = 5$. The actual sizes of the particles are scaled down by a factor of 0.075. Each super-quadric is discretised by a surface triangular mesh with 400 vertices and 796 elements. A golden spiral scheme [12] is adopted here to generate the triangular mesh, although a mesh reduction technique [12] could be applied to optimally reduce the mesh size.

The three particles are positioned in a cubic box with side of 0.8m. Initially, the top particle is given a unit downward velocity, while the other two are stationary. The mass density is set to be $2000kg/m^3$. A linear contact model with $k_n = 10^6 N/m$ is applied to all contacts including particle-wall contacts. No damping or friction is considered, but gravity is included.

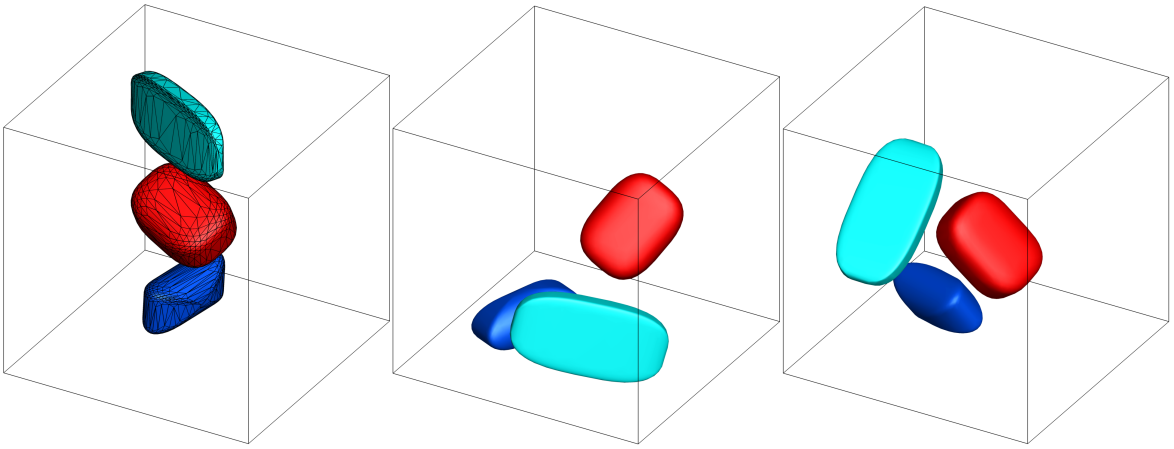

(a) Initial position (b) An intermediate position (c) Final position

Figure 7: Configurations of three super-quadric particles during an elastic impact at different time instances

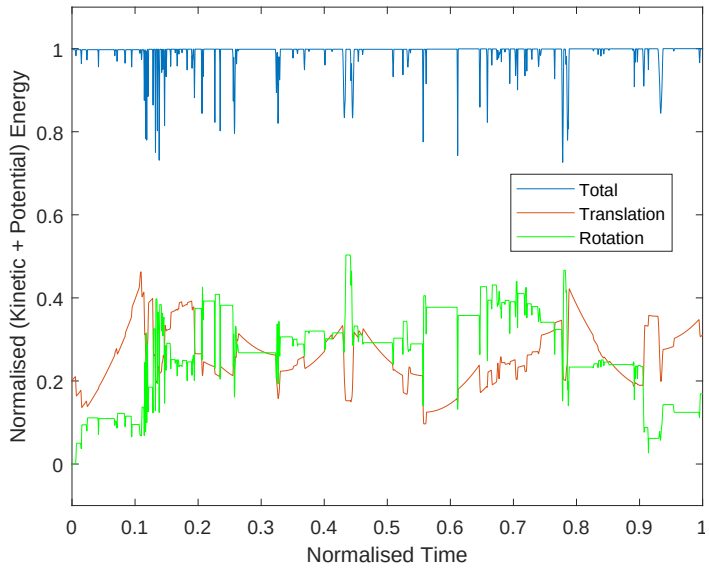

Figure 8: The evolution of the total, translational and rotational energies of the three super-quadrics. The total energy includes the potential energy.

The time step is set to be $= 1.25 \times 10^{-5} s$, and the total number of time integration steps is 100,000, so the whole simulation covers 1.25s.

Under the action of gravity and also the non-zero velocity of the top particle, the particles start to move and elastic impact occurs among the particles and also between the particles and the four walls of the box. Figures 7(b) and (c) show the positions of the particles at two stages.

At each time instant, the total translational and rotational kinetic energies, and the total energy (including the potential energy) of the system are recorded. The evolution of these three energies is shown in Figure 8, where they are normalised by the maximum total energy. Each drop of the total energy corresponds to one elastic collision event. In the whole impact duration considered, there are about 85 individual collisions occurred. The relative difference between the initial total energy and the maximum total energy is 0.002. This indicates that

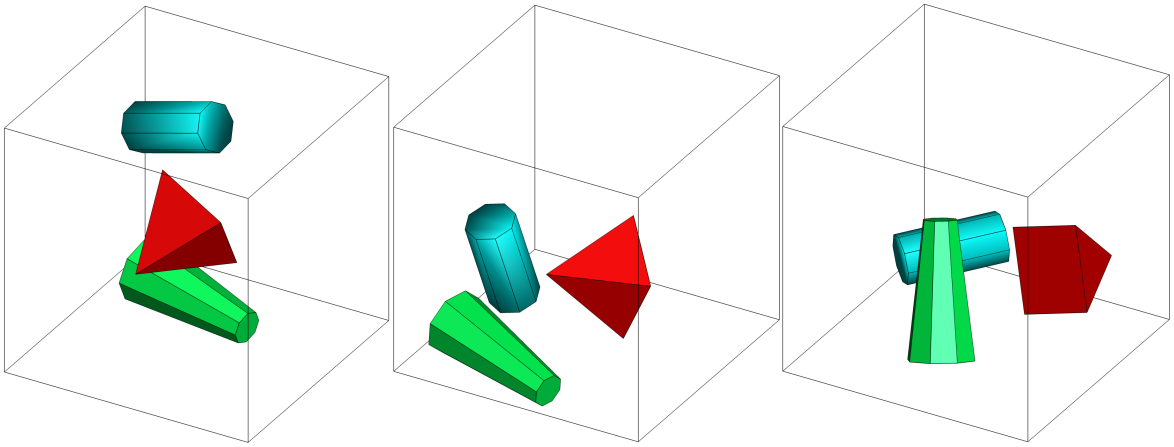

(a) Initial position (b) An intermediate position (c) Final position

Figure 9: Configurations of three polyhedral particles during an elastic impact at different time instances

that energy conservation is indeed maintained as theoretically guaranteed by the Minkowski overlap based contact model.

Verification 2: Elastic impact of three polyhedra.

This example consists of three polyhedral particles as shown in Figure 9(a) in the initial positions. Except for the shapes and sizes of the particles, anything else is the same as in the previous case. As more sharp edges and corners are presented, a significant change of contact features between two consecutive steps could be more easily encountered in the simulation. Thus this example provides a tougher case to test the energy-conserving property of the proposed Minkowski based methodology.

The evolution of the three energies of the system is shown in Figure 10, where they are normalised by the maximum total energy. Again in the whole impact duration considered, there are more than 80 individual elastic collisions occurred. The relative difference between the initial total energy and the final total energy is 0.003 which is slightly larger than the previous case. This indicates again that energy conservation is preserved in this example.

5.2 Illustrative Simulations

Two illustrative simulations of particles randomly deposited into a box with dimensions of $5 \times 5 \times 15m$ are presented below. All contacts are frictional with the coefficient of friction set to be 0.5, and the standard Coulomb friction model is used to account for friction in the tangential direction. A coefficient of restitution equal to 0.1 is also applied to both normal and tangential contacts. Other modelling parameters are the same as the two verification examples above. Another application of the methodology to discrete element modelling of rockfill systems used for structural protection under high speed projectile impact can be found in [23].

Simulation 1: Packing of super-quadric particles.

This simulation randomly generates and deposits 987 super-quadric particles into the box within the time interval $t \in [0, 2.5]s$. The particles are scaled versions of the three particles used in Verification 1. The injected particles are allowed to settle until $t = 5s$.

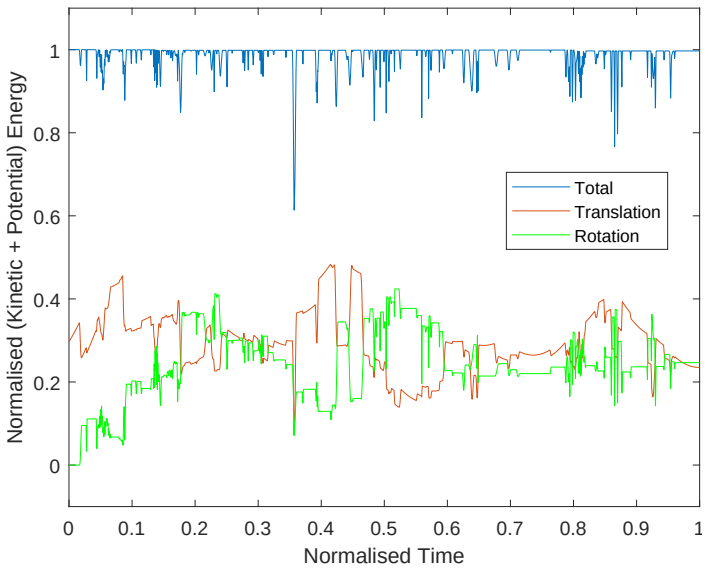

Figure 10: The evolution of the (normalised) total, translational and rotational energies of the system. The total energy includes the potential energy.

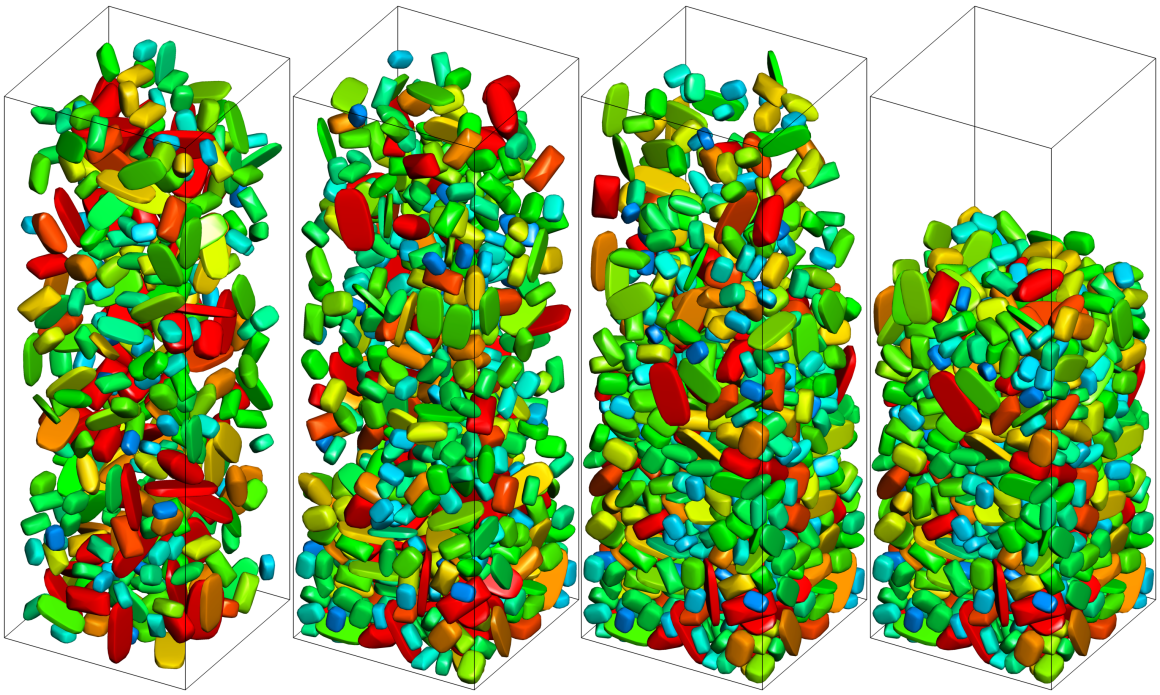

(a) t = 0.25s (b) t = 1.25s (c) t = 2.50s (d) t = 5.0s

Figure 11: Simulation 1 - Configurations of the 3-type super-quadric system at four time instants

The packing configurations of the system at four time instances are depicted in Figure 11. A stable packing is achieved at the end of the simulation.

Simulation 2: Packing of polyhedral and super-quadric particles.

In this simulation, particles scaled from the three polyhedra used in Verification 2 are mixed with some particles scaled from the second super-quadric in Verification 1. In total, 3280

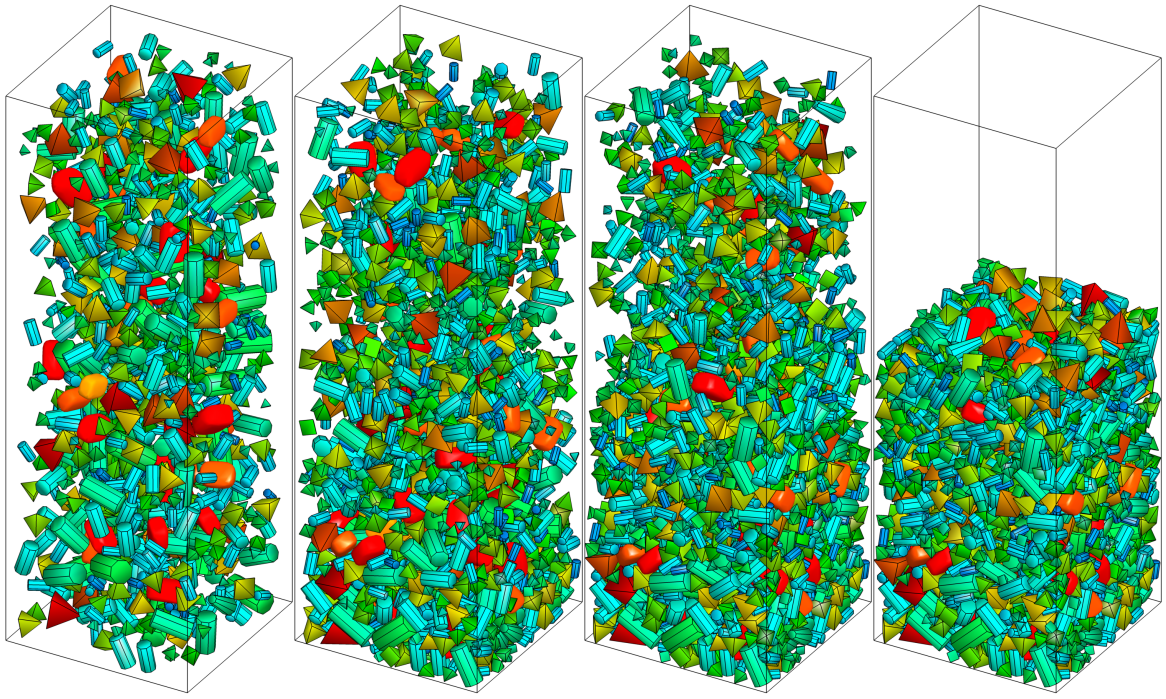

(a) t = 0.25s (b) t= 1.25s (c) t = 2.5s (d) t = 5.0s

Figure 12: Simulation 2 - Configurations of the 3-type polyhedra + discretised super-quadric system at four time instants

particles are randomly generated and deposited in $t \in [0, 2.5]s$, and settled until $t = 5s$.

The packing configurations of the system at four time instances are depicted in Figure 12. A stable packing is observed again at the end of the simulation.

In the above two simulations, no detailed analysis of the performance of GJK and EPA is conducted. Such analysis can be found in [13] where the average GJK and EPA iterations for different contact groups at different stages of the packing are provided.

6 Concluding Remarks

Based on the Minkowski difference of two shapes and the equivalence between the contact state of the two shapes and the location of the origin relative to their Minkowski difference, the Minkowski overlap has been proposed which provides a unified definition of the contact overlap between any two shapes, either convex or concave. The corresponding Minkowski contact features have also been defined. A unique property of the Minkowski overlap has also been introduced which forms the theoretical foundation for the proposed Minkowski overlap based energy-conserving contact model. A rigorous reasoning has also been provided to ensure that this energy conservation property is still held for cases where contact normals and points may undergo discrete changes. For convex particles, the computational procedure combining both GJK and EPA algorithms has proved to be very robust and effective if a support point can be explicitly defined for each geometric shape involved. When such an explicit expression is not available for a shape, a surface triangular mesh approximation can always be applied to convert the shape into a convex polygons/polyhedron. The uniqueness and ambiguity issues that may arise in determining the contact features of a contact in special

cases have been clarified and fully resolved.

The elastic energy conservation of two convex shapes for an elastic impact has also been numerically verified using two examples, while two more examples involving more particles with different sizes and shapes have been conducted to further demonstrate the robustness and applicability of the proposed computational procedure and the Minkowski overlap contact model.

As mentioned previously, although the Minkowski overlap and the energy-conserving contact model proposed are applicable to both convex and concave and therefore are universal, the two main computational procedures, GJK and EPA, outlined and employed for the numerical examples in this work are for convex shapes only. Computational procedures suitable for concave shapes are much more complex and will be proposed elsewhere.

Also note that no verification and validation of the actual contact energy function which leads to compute the contact force magnitude has been made. This is a physically very important issue, but common to all non-spherical contact models. More work will be needed in this aspect in general.

Acknowledgement

This work is partially supported by National Natural Science Foundation of China under Grant Nos. 12072217 and 11772135, and by Open Fund of State Key Laboratory of Coal Resources and Safe Mining, China University of Mining and Technology, Beijing, China [Grant No. SKLCRSM19KFA12]. All the support is gratefully acknowledged.

Data Availability Statement

The data that support the findings of this study are available from the corresponding author upon reasonable request.

References

[1] P. A. Cundall, and O. D. L. Strack. A discrete numerical model for granular assemblies. *Geotechnique*, 29(1):47-65, 1979.

[2] S. Ji. and L. Lu. *Computational Granular Mechanics and Its Engineering Applications.* Springer, 2020. ISBN 978-981-15-3304-4.

[3] P. A. Cundall. Formulation of a three-dimensional distinct element model - Part I. A scheme to detect and represent contacts in a system composed of many polyhedral blocks. *Int. J. Rock Mech. Min. Sci. & Geomech.*, 25:107-116, 1988.

[4] Y. T. Feng, K. Han, D. R. J. Owen. A generic contact detection framework for cylindrical particles in discrete element modelling. *Comput. Methods Appl. Mech. Engrg.* 315:632-651, 2017.

[5] S. Wang, Y. Fan, S. Y. Ji. Interaction between super-quadric particles and triangular elements and its application to hopper discharge. *Powder Technology.* 339:534-549, 2018.

[6] C. Wellmann, C. Lillie and P. Wriggers. A contact detection algorithm for superellipsoids based on the common-normal concept *Engineering Computations.* 25(5):432442, 2008.

[7] M. A. Hopkins. Discrete element modeling with dilated particles. *Engineering Computations,* 21(2/3/4):422-430, 2004.

[8] L. Liu, S. Ji. Bond and fracture model in dilated polyhedral DEM and its application to simulate breakage of brittle materials. *Granular Matter*, 21, Article No. 41, 2019. doi:10.1007/s10035-019-0896-4

[9] Y. T. Feng. An energy-conserving contact theory for discrete element modelling of arbitrarily shaped particles: Basic framework and general contact model. *Comput. Methods Appl. Mech. Engrg.* 373:113454, 2021.

[10] Y. T. Feng. An energy-conserving contact theory for discrete element modelling of arbitrarily shaped discrete elements: Contact volume based model and computational issues. *Comput. Methods Appl. Mech. Engrg.* 373:113493, 2021.

[11] Y. T. Feng. A Generic Energy-Conserving Discrete Element Modelling Strategy for Concave Particles Represented by Surface Triangular Meshes *Int. J. Numer. Methods in Engrg.* 2021;117. https://doi.org/10.1002/ nme.6633.

[12] Y. T. Feng. An Effective Energy-Conserving Contact Modelling Strategy for Spherical Harmonic Particles Represented by Surface Triangular Meshes with Automatic Simplification. *Comput. Methods Appl. Mech. Engrg.* 379:113750, 2021.

[13] Y. T. Feng, Y. Tan. On Minkowski difference-based contact detection in discrete/ discontinuous modelling of convex polygons/polyhedra: Algorithms and implementation. *Engineering Computations.* 37:54-72, 2020.

[14] E. G. Gilbert, D. W. Johnson and S. S. Keerthi. A Fast Procedure for Computing the Distance between Complex Objects in Three-Dimensional Space. *IEEE Trans. Robotics and Automation.* 4(2):193-203, 1988.

[15] G. van de Bergen. Proximity queries and penetration depth computation on 3d game objects. Game Developers Conference, 2001.

[16] Y. T. Feng, W. Gao. On the strain energy distribution of two elastic solids under smooth contact *Powder Technology.* 389:376-382, 2021.

[17] T. M. Apostol. *Calculus, Vol. 1: One-Variable Calculus with an Introduction to Linear Algebra.* (2nd ed.), New York: John Wiley & Sons, 1967. ISBN 978-0-471-00005-1.

[18] G. H. Shi. Basic equations of two and three dimensional contacts. Proceedings of the 47th US Rock Mechanics/Geo-mechanics Symposium, San Francisco, ARMA: 253-269, 2013.

[19] G. H. Shi. Basic theory of two dimensional and three dimensional contacts. Frontiers of Discontinuous Numerical Methods and Practical Simulation in Engineering and Disaster Prevention, Taylor & Francis Group, London, 2013.

[20] C. Cameron. Enhancing GJK: Computing Minimum and Penetration Distances between Convex Polyhedra. *Int Conf Robotics and Automation*, pages 3112-3117, April 1997.

[21] A. H. Barr. Superquadrics and Angle-Preserving Transformations. *IEEE Computer Graphics and Applications.* 1(1):11-23, 1981.

[22] A. Dullweber, B. Leimkuhlera and R. McLachlanb. Symplectic splitting methods for rigid body molecular dynamics. *J. Chem. Phys.* 107(15):5831-5851, 1997.

[23] T. Zhao, Y. T. Feng, J. Zhang, Zhihua Wang, Zhiyong Wang. Discrete Element Modelling of Dynamic Behaviour of Rockfills for Resisting High Speed Projectile Penetration. *Computer Modeling in Engineering & Science* 127(2):721-735, 2021.

Appendix A: GJK

1. Input: Two shapes A and B
2. Initialisation
    a. Set Simplex $\mathbf{S}$ to be empty: $\mathbf{S} = \varnothing$
    b. Choose an (arbitrary) initial search direction $\mathbf{v} \neq 0$
3. Iteration
    a. Compute the support point $\mathbf{a} = \mathbf{p}_s(A \ominus B, \mathbf{v})$
    b. If $\mathbf{a} \cdot \mathbf{v} < 0$, **stop** $\mathbf{S} = \varnothing$ (NO CONTACT)
    c. Update Simplex $\mathbf{S}$
        i. Add $\mathbf{a}$ to $\mathbf{S}$ as a new vertex
        ii. If $\mathbf{S}$ contains the origin $\mathbf{o}$, **stop S** (CONTACT);
        iii. Reduce $\mathbf{S}$ to the lowest dimension possible that still contains the closest feature to the origin by discarding vertices.
        iv. Compute a new search direction $\mathbf{v}$ that is towards the origin normal to the new simplex; and go to 3.a
4. Output: Simplex $\mathbf{S}$

Appendix B: EPA

1. Input: Two shapes A and B; Simplex $\mathbf{S}$ outputted from GJK
2. Initialisation
    a. Take the simplex $\mathbf{S}$ returned from the GLK algorithm as the start polytope $\mathbf{P} = \mathbf{S}$.
    b. Expand $\mathbf{P}$ to be a full simplex by adding new vertices if $\mathbf{S}$ is a degenerated simplex.
    c. Compute the distance d_i of each face $i \in \mathbf{P}$ to the origin.
3. Iteration
    a. Find the closest face $f \in \mathbf{P}$ to the origin $\mathbf{o}$, and set the search direction to be $\mathbf{n}_f$, where $\mathbf{n}_f$ is the outward normal of the closest face f. Let d_f be the distance of the face f to the origin.
    b. Compute the support point $\mathbf{a} = \mathbf{p}_s(A \ominus B, \mathbf{n}_f)$
    c. Compute the distance between $\mathbf{a}$ and the origin $\mathbf{o}$ along the direction $\mathbf{n}_f$: $d_a = \mathbf{n}_f \cdot \mathbf{a}$
    d. Check for convergence: if $d_a - d_f < \epsilon$ (given tolerance), **go to 4**

e. Expand $\mathbf{P}$:
For each face $f \in \mathbf{P}$ which is *visible* from $\mathbf{a}$, i.e. $\mathbf{n}_f \cdot (\mathbf{a} - \mathbf{v}_f) > 0$ (where $\mathbf{v}_f$ is any vertex of the face)
   i. Remove the face f from $\mathbf{P}$
   ii. Add new faces formed by the vertices of the face and the new point $\mathbf{a}$ to $\mathbf{P}$; and calculate the distance of each new face to the origin.

f. Go back to 3.a

4. Compute Contact Features

   a. Find the projected point $\mathbf{c}$ of the origin $\mathbf{o}$ on the closest face f.

   b. Set Contact overlap $\delta_M = d_f$, and compute Contact normal $\mathbf{n}_M = \mathbf{c}/\delta_M$

   b. Compute Contact points on the two shapes
      i. Compute the local or barycentric coordinates $\boldsymbol{\xi}_c$ of $\mathbf{c}$ in the face using its vertices
      ii. Assume the same local $\boldsymbol{\xi}_c$ on the corresponding face of each shape to compute the local point contact $\mathbf{c}_k, (k = 1, 2)$
      iii. Compute the common contact point $\mathbf{c}_M = (\mathbf{c}_1 + \mathbf{c}_2)/2$

5. Output: Contact Features $\delta_M, \mathbf{n}_M$ and $\mathbf{c}_M$